Materials & Design 265 (2026) 115852

Contents lists available at ScienceDirect

Materials & Design

journal homepage: www.elsevier.com/locate/matdes

Pre-processing history dependent foaming behavior and morphing of thermoplastic polyurethane

Lorenzo Miele[a,b,1], Emilia Di Lorenzo[a,b,1], Denise Bellisario[c,d], Ernesto Di Maio[a,b,*]

[a] Dipartimento di Ingegneria Chimica, dei Materiali e della Produzione Industriale, University of Naples Federico II, P.le Tecchio 80, Naples, 80125, NA, Italy
[b] foamlab, University of Naples Federico II, P.le Tecchio 80, Naples, 80125, NA, Italy
[c] Department of Industrial Engineering, University of Rome Tor Vergata, Via del Politecnico 1, Rome, 00133, RM, Italy
[d] Dipartimento di Ingegneria e Scienze, Universitas Mercatorum, Piazza Mattei, 10, Rome, 00186, RM, Italy

HIGHLIGHTS

- Foamability of 3D printed, neat and loaded, TPU is compared to as-received granules.
- Pre-processing history critically controls foam density, morphology and shrinkage.
- Microstructural tailoring controls gas transport and foaming.
- Exploitation of local differences in foamability leads to foam-induced morphing.

GRAPHICAL ABSTRACT

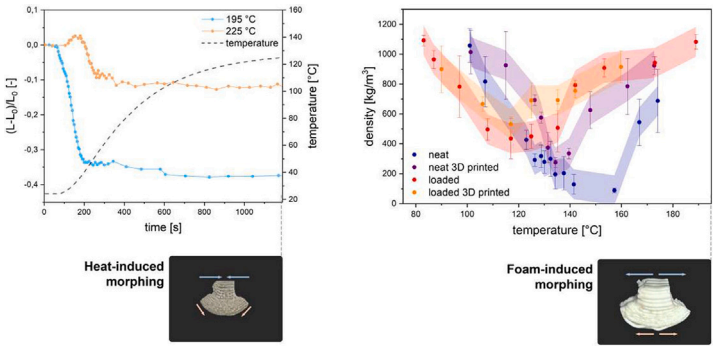

ARTICLE INFO

Keywords:
Foam
Thermoplastic
Shrinkage
Elastomer
3D printing

ABSTRACT

Thermoplastic polyurethanes (TPUs) foams are valued for their low density, energy absorption, low thermal conductivity, and, in general, tunable properties. These features make them ideal for applications such as sportswear, flexible electronics, shape memory sensors, and soft robotics. Foaming of thermoplastic polymers is highly affected by the state of the polymer in terms of molecular chain arrangement, crystallinity, and residual stresses, which, in turn, are strongly influenced by the pre-processing history of the material. These complexities, together with multiphase morphology, make TPU foaming particularly challenging for achieving high expansion ratios. Preforms with different thermal and deformation histories are here selected to serve as models for exploring the relationship between pre-processing and foaming, with and without the addition of fillers. We analyze the expansion ratio, foam morphology, microstructural features, and post-foaming shrinkage of neat TPU, 3D-printed TPU structures, and TPU composites with multi-walled carbon nanotubes and aluminum nanoparticles using the batch foaming technique under varying processing conditions. Results show the critical role of pre-processing (in terms of printing parameters) and addition of fillers in influencing the foamability, and highlight microstructural control through pre-processing as a key strategy to tailor TPU foams for advanced structural and functional applications. Building on this, we introduce foam-induced morphing, validating mold-free batch foaming as a tool for designing lightweight systems with precisely tuned mechanics and morphing behaviors

* Corresponding author at: Dipartimento di Ingegneria Chimica, dei Materiali e della Produzione Industriale, University of Naples Federico II, P.le Tecchio 80, Naples, 80125, NA, Italy.
Email address: edimaio@unina.it (E. Di Maio).

[1] These authors contributed equally to this work.

https://doi.org/10.1016/j.matdes.2026.115852
Received 11 December 2025; Received in revised form 2 March 2026; Accepted 13 March 2026
Available online 19 March 2026

1. Introduction

Thermoplastic polyurethane (TPU) foams are lightweight, flexible, and durable materials, striking a good balance between strength and impact resistance. Their key properties, including high elastic deformability and resilience, excellent energy absorption, and customizable structural and functional behavior, make them suitable for many applications such as sporting goods, flexible electronics, shape memory sensors, and soft robotics [1–3]. These emerging applications increasingly require foams with complex geometries, advanced structures, non-uniform density, and functional properties [4,5].

When it comes to the production of foams with this level of complexity, conventional molding technologies, such as foam injection molding, steam chest molding, and foam compression molding, are not well suited. Although these methods are well established for manufacturing uniform, mono-material products [1], they inherently limit design flexibility, scalability, and cost-effectiveness, particularly when dealing with complex geometries, non-uniform properties, customized designs, or small-batch production [6–9].

A promising alternative is the use of a mold-free foaming technology, in which the final shape and functionality of the product can be imposed prior to foaming through the design of a preform. The limitations imposed by rigid molds are thus bypassed, in favor of design flexibility and ease of customization. However, to ensure that the shape integrity of the preform is maintained, the foaming process must occur below the polymer melting temperature [10]. Hence, the successful implementation of this strategy requires a coupled design of both the preform and the mold-free foaming process.

Among the available techniques, batch foaming stands out as an effective method for processing designed preforms into foamed parts, without the need for melting or remolding. This process involves solubilization of a physical blowing agent into the preform at high temperature followed by rapid depressurization, promoting cell nucleation and growth [11]. Provided the process occurs below the melting temperature, the geometry of the initial shape is maintained, to a certain extent.

Examples of such a combined approach have been proposed in literature, and they include batch foaming, or foam compression molding, of complex-shaped preforms fabricated either with injection molding [12] or with the 3D printing technology [13,14]. Nevertheless, the relationship between preform design and the resulting foam properties has not yet been investigated.

The production of TPU foams is not trivial, as TPU poses intrinsic challenges during the foaming process. Its unique molecular architecture, which is that of a block copolymer composed of alternating soft segments (SSs) and hard segments (HSs) [15], introduces complexities such as post-foaming shrinkage, low melt strength, and complex crystallization behavior [1]. Indeed, the presence of SSs and HSs determines the formation of a complex crystalline microstructure [16,17], which influences the polymer properties in terms of rheological behavior [18], sorption thermodynamics, and mass transport properties [19]. This, in turn, directly impacts the foaming process, affecting bubble nucleation, growth dynamics, and foam stability, as extensively reported in the literature for semi-crystalline homopolymers like polylactic acid (PLA) or polypropylene (PP). In these cases, crystallinity follows a predictable development path, resulting in a single dominant crystalline phase whose presence significantly influences key factors, including the expansion ratio [20], the efficiency of heterogeneous nucleation [21], and the resulting cell morphology [22]. As a consequence, tuning the polymer crystalline phase, either prior to, or during the foaming process, stands out as an important additional parameter to control foamability.

For the complex case of TPUs, still few studies have analyzed the link between microstructure and foamability, but some conclusions have been reached demonstrating that the final foam characteristics are not determined solely by the foaming conditions but also by the microstructural state of the preform [20,23,24]. Indeed, thermal, mechanical, or printing processing of the preform can affect segmental mobility, phase separation, and crystallinity modifications, all of which influence foam expansion and stability.

Choosing suitable printing parameters was identified as the key to achieving high-quality 3D printed parts [25,26]. Many studies on manufacturing parameters, such as printing speed, printing temperature, build plate temperature, build orientation, layer thickness, raster angle, infill pattern, and infill density, have been published in the literature [25,27,28], and their effect on the mesostructure, mechanical properties, thermal profile and stress build-up of the 3D printed part has been widely proven [28], thus confirming them as a powerful tool to improve quality, mechanical strength and microstructure of prints [25].

Beyond microstructural effects, when functional properties are required, the incorporation of fillers or functional additives provides an additional factor affecting TPU foamability. Fillers such as carbon nanotubes (CNTs), nano-clays, or silica particles can act as nucleating agents, promoting heterogeneous cell nucleation, resulting in a more uniform cell morphology [29]. Their presence can also stabilize cell walls and mitigate common critical issues of TPU foaming, including shrinkage and low melt strength [30]. On the other hand, additives often reduce chain mobility, leading to a reduction in the maximum expansion ratio compared to neat TPU [31]. As a result, fillers play a dual role: while they may limit overall foam growth, they enable a more controlled morphology and improved dimensional stability, which are key for functional applications.

This study focuses on analyzing and leveraging the effect of pre-processing on TPU foamability under various foaming conditions. More specifically, the 3D printing technology, specifically tuned by changing key printing parameters, is used to produce preforms with defined geometry, as well as thermal and deformation histories, with and without the addition of multi-walled carbon nanotubes (MWCNTs) and aluminum nanoparticles (AlNPs) as fillers, to serve as models for exploring the relationships between pre-processing and the final foam properties. The impact of different pre-processing routes is thus explored, specifically in terms of density reduction, cell morphology, post-foaming dimensional stability (i.e., shrinkage), and 3D printing geometry. Understanding how the processing history of the preform influences the final foam properties offers a powerful design tool for tailoring TPU foams.

Advantages associated with the combined use of pre-processing and mold-free technology are also taken into account. The possibility of having no constraints during foam expansion, together with the ability to tailor both sample geometry and processing history, allows us to design predefined shape transitions that can only be triggered by the foaming process: new routes of polymer morphing are introduced and explored.

2. Materials and methods

2.1. Materials

Commercial TPU pellets (DiAPLEX MM3510, Ether Type), with a density (ρ_{TPU}) of 1250 kg/m^3 were purchased from SMP Technologies Inc, Tokyo, Japan; MWCNTs (outer diameter < 8 μm, length 10–30 μm, purity > 95 wt% and ash < 1.5 wt%) were purchased from CHEAPTUBES.COM. AlNPs (diameter 40–60 nm) were purchased from US Research nanomaterials, Houston, Texas, United States. The products were used as received, without any purification process. The blowing agent (BA), CO_2 (purity 99.99%), was supplied by SOL S.p.A., Monza, Italy.

2.2. Methods

2.2.1. Preforms preparation

TPU composites loaded with a mixture of MWCNT and AlNP were prepared using a Brabender Plastograph mixer (Anton Paar, Graz, Austria) by melt-mixing TPU pellets with a total of 3 wt% of MWCNTs and AlNPs in a 5:1 ratio. Mixing was performed at 150 °C for a total of 10 min (3 min for the neat polymer and 7 min after filler addition) at

a rotation speed of 50 rpm. Both neat TPU and the resulting composite were extruded into filaments with a diameter of 1.75 ± 0.1 mm using a filament maker (Composer 450, 3DEVO, Utrecht, Netherlands). These filaments were then used to fabricate square-shaped samples via 3D printing using a commercial fused deposition modeling (FDM) printer (Prusa i3 MK3S + , Prusa Research, Prague, Czech Republic), with a nozzle temperature (T_{print}) ranging from 195 to 225 °C, a bed temperature of 50 °C, and a printing speed (v_{print}) ranging from 10 to 40 mm/s. Further details on the composite preparation and printing process are provided elsewhere [32]. To evaluate the shape morphing, a two-layer beam shaped structure measuring 1 cm in width and 5 cm in length, with a thickness of 1 mm, was produced. The first layer was printed at 225 °C and 20 mm/s, while the second layer was printed at 195 °C and 20 mm/s.

2.2.2. Foaming experiments

Both the TPU pellets and the 3D printed samples were subjected to a foaming process using batch foaming technology, employing custom made batch foaming equipment described in detail elsewhere [33]. This consists of a pressure vessel heated by thermoresistor elements, capable of heating up to 350 °C, and equipped with a pressure control system that allows for regulation of pressure up to 200 bar. The system enables the use of several types of blowing agent and it allows for the control of the pressure drop rate (*PDR*) up to 10'000 bar/s, enabling the application of various foaming strategies. Moreover, the use of a sapphire glass window enables in situ monitoring of the polymer sample expansion.

The samples were loaded into the pressure vessel at the set temperature under vacuum conditions for 15 min. The vessel was then filled with CO_2 at the desired pressure (ranging from 120 to 170 bar). The pressure was maintained constant for a saturation time (t_{sat}) of 15 min, after which it was rapidly released, with a *PDR* ranging from 50 to 933 bar/s [33]. The tests were performed at various treatment temperatures, ranging from 83 °C to 170 °C. Each experiment was repeated at least three times to allow for statistical analysis.

2.2.3. Density measurement

The density of the foamed samples was measured immediately after the foaming process using a density kit mounted on a laboratory balance (MS104S/01, Mettler Toledo, Columbus, Ohio).

Considering the balance readings in air and in water (w_{air} and w_{water}, respectively), the foam density (ρ_{foam}) was evaluated as:

$$\rho_{foam} = \frac{w_{air}}{w_{air} - w_{water}}. \tag{1}$$

2.2.4. Differential scanning calorimetry

The influence of both pre-processing and foaming processes on the thermal properties and microstructure of the material was evaluated by differential scanning calorimetry (DSC) using a Discovery 250, TA Instruments, New Castle, Delaware, United States. The samples were heated from 20 °C to 220 °C at a rate of 10 °C/min, and the resulting peak positions and integrals were analyzed with the TRIOS software (TA Instruments, New Castle, Delaware, United States). The crystal melting peaks and the heat enthalpy required to melt the crystals (δH) were thus identified and quantified.

2.2.5. Rheological characterization

The rheological characterization was performed using an ARES rotational rheometer (TA Instruments, New Castle, Delaware, United States). Disk shaped samples were loaded at ambient temperature and immediately brought to 100 °C, then a temperature sweep test was performed at a constant strain of 0.1% (within the linear viscoelastic regime) and at an angular frequency of 1 rad/s, with a temperature ranging from 100 °C to 190 °C. Afterward, to address the effect of pre-processing, different cooling ramps (from melt), namely at 1, 5, and 10 °C/min, were performed. In between each cooling ramp, a heating ramp at 10 °C/min up to 190 °C was carried out to bring the sample back to the melt state. Moreover, a frequency sweep test was carried out on both the neat and loaded TPU at a constant temperature of 120 °C and a strain of 0.1% with an angular frequency ranging from 0.1 to 100 rad/s. The rheological behavior was evaluated by monitoring the storage modulus (G') and loss modulus (G'') as a function of temperature.

2.2.6. Morphology characterization

The morphology of the TPU foams was examined through Scanning Electron Microscopy (SEM, TM3000, Hitachi High-Technologies Corporation, Tokyo, Japan) after sputter-coating the samples with a thin layer of platinum to enhance surface conductivity. Bubble average size (ϕ) and bubble size distribution were determined using the software ImageJ [34]. Bubble number density (N) was determined using the following equation:

$$N = \left(\frac{n}{A}\right)^{3/2} \times \frac{\rho_{TPU}}{\rho_{foam}}, \tag{2}$$

where n is the number of cells and A is the total sample area visible in the SEM image.

2.2.7. Shrinkage evaluation

The shrinkage behavior of the TPU foams was evaluated by measuring the density of all the samples seven days after the foaming process (ρ_{shrink}), during which they were stored at room temperature. The shrinkage % ratio (SR) was calculated as follows:

$$SR = \frac{\rho_{shrink} - \rho_{foam}}{\rho_{foam}} \times 100. \tag{3}$$

2.2.8. Thermal shrinkage evaluation

The thermal shrinkage of the 3D-printed samples was evaluated by measuring the length change of a 3D printed strand when heated from room temperature to 134 °C at a rete of almost 5 °C/min. Two 3D printed strands were produced at 195 °C and 225 °C, and then treated in the aforementioned pressure vessel (Section 2.2.2) under vacuum. A sapphire window and a high resolution CCD camera (BV-7105H, Appro equipped with a modular zoom lens system, Zoom 6000, Navitar) were used to in situ monitor the sample shape over time. A snapshot of the filament was taken every 5 s and shrinkage was evaluated by measuring the filament length over time using the ImageJ software. To compare the behavior of the two filaments, we estimated the ratio $(L - L_0)/L_0$, where L_0 is the initial length of the 3D-printed strand and L the corresponding length after the thermal treatment.

3. Results and discussion

We hereby explore the foaming behavior of 3D printed TPU, with and without the addition of fillers, examining how the microstructural modifications introduced before foaming can influence the final foam density, morphology and shrinkage. Indeed, since the preform is not brought to a molten state during the foaming process, the thermal and mechanical history of the preform plays a crucial role in influencing material processing and subsequent expansion. To assess this effect, we performed experiments under identical foaming conditions on both TPU pellets and 3D printed TPU preforms obtained (i) at varying printing parameters (i.e., T_{print} and v_{print}) and (ii) with the addition of fillers, as this proved to be an effective way to alter the thermal properties and the morphology of the material.

3.1. Effect of filler addition

3.1.1. Thermal analysis

Analysis of the DSC curves of neat TPU (pellets and 3D printed preforms) and loaded TPU (filaments and 3D printed preforms) reveals differences in the scan of each preform type (Fig. 1a), confirming that

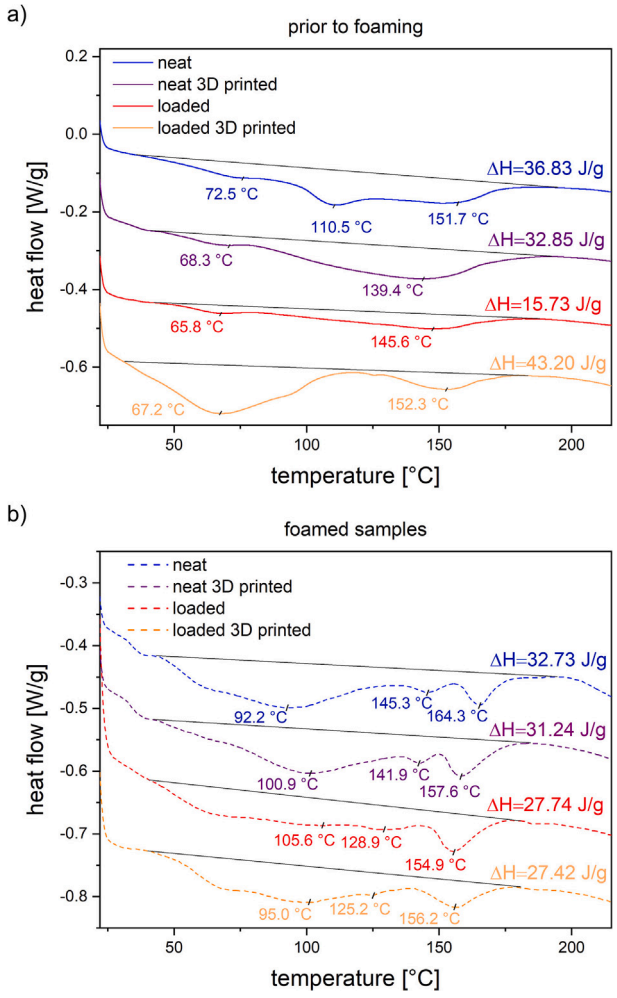

Fig. 1. DSC curves of each preform type: (a) prior to foaming, and (b) after foaming under the same processing conditions.

modifications introduced before foaming are effective in modulating the microstructure.

All samples exhibit multiple endothermic peaks, characteristic of the complex melting behavior of TPUs [35,36]. Despite the interpretation of the origin of these peaks still being under debate for TPU [17], some conclusions about the microstructure can be drawn. The low-temperature peak corresponds to the melting of the less ordered HS regions, resulting from the annealing process, whereas the high-temperature peaks arise from the melting of the more ordered, para-crystalline or micro-crystalline HS crystal phases [37,38].

As visible from Fig. 1(a), the neat TPU displays three well-defined peaks, while the other preforms show a broader peak either at high (for the neat 3D printed and the loaded preforms) or at low temperature (for the loaded 3D printed preform), indicating the presence of different, more polydisperse crystal domains [17].

This is evident from the DSC of the 3D printed preform (purple curve) in which the merging and broadening of the high-temperature peaks resemble partial annealing [37]. Something similar is observed in the case of the loaded preform (red curve), but with a reduced ΔH, reflecting an overall reduced crystallinity. Finally, the loaded 3D printed preform shows the highest ΔH value.

The differences in the microstructure are still visible after the foaming process (Fig. 1b). Indeed, all the samples exhibit a comparable DSC profile, with a sharper high-temperature peak, a broader low-temperature peak, and an intermediate transition, consistent with the development of a complex crystalline structure [39]. However, variations in peak position and enthalpy persist, demonstrating that the foaming treatment does not fully erase the differences in preform microstructure, differences that, in turn, severely affect the foam formation, as they influence gas solubility, bubble nucleation and growth processes, hence foam morphology, and structural stability [19–21].

3.1.2. Rheological analysis

The effect of different pre-processing treatments was explored through rheology, via application of different cooling and heating ramps on the neat material (Figure SI 1) and through frequency sweeps on the neat and loaded samples. Fig. 2 shows the effect of fillers on TPU rheology. Here, the loaded sample presents higher moduli values, denoting a higher complex viscosity, as typically occurs in the presence of fillers. This result is apparently in contrast with the one from Fig. 1(a), which indicates a lower overall crystallinity in the case of loaded samples. This inconsistency suggests that the different microstructure, supported by the DSC measurements, is not directly linked to the material rheology, despite still having a significant impact on foamability as it severely affects gas solubility and diffusivity [19].

3.1.3. Foaming window

The foamability of each preform type is evaluated by the density measurements of the samples collected right after the foaming process at different foaming temperatures (Fig. 3). Among all the preforms, the neat TPU shows the largest density reduction and the broadest foaming window, with a minimum density of 88 ± 15 kg/m^3 at 157 °C. Conversely, the neat 3D printed preform shows a reduced foaming window (129–148 °C), and a higher minimum density of 329 ± 14 kg/m^3. Regarding the loaded preforms, the foam density is always higher than that of the neat counterparts at a fixed temperature. This is related to the increase in the material viscosity shown in Fig. 2(c), which hinders bubble growth. Also, the foaming window is shifted toward lower temperatures, which is a non-trivial result, again linked to the high viscosity, but also to the change in the microstructure.

From the density map, we can notice that changing the preform, i.e., using a TPU sample with a different pre-processing history, affects the final foam density even when the foaming conditions remain unchanged. As an example, when foaming the neat TPU and the 3D printed preform at 160 °C, we obtain samples with two very different densities. This result may be employed and exploited for the production of advanced mono-material foam products (see Section 3.3).

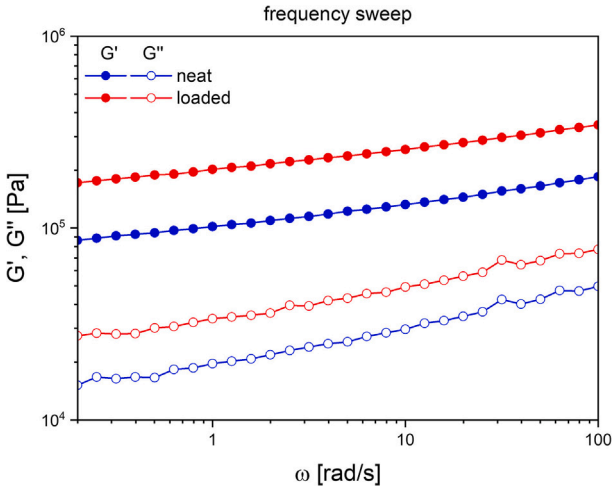

Fig. 2. Superimposed storage modulus (G', solid symbols), and loss modulus (G", open symbols), at a constant strain of 0.1% as a function of frequency, at 120 °C, for neat and loaded TPUs.

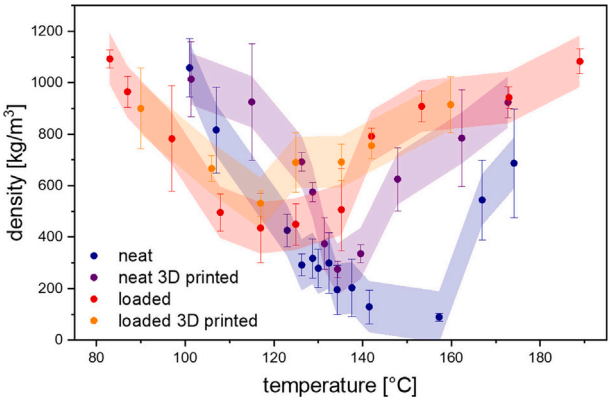

Fig. 3. Effect of foaming temperature on density reduction for different preforms processed by batch foaming at a pressure of 120 bar of CO_2 and a PDR of 933 bar/s.

The effect of pressure and PDR was also explored by performing foaming experiments at 134 °C, i.e., the optimal foaming temperature for the neat 3D printed sample.

Results of the pressure sweep are shown in Fig. 4(a) for three different preforms. The neat TPU shows the best foamability across the entire pressure range, with a negligible pressure dependence; conversely, the neat 3D printed and loaded preforms show a lower foamability compared to the neat TPU—as already evidenced by the temperature sweep—with a similar dependence on pressure: in both cases, foam density increases as pressure increases, identifying the best foaming pressure at 120 bar. This behavior is non-trivial, since higher pressures, typically, either enhance gas solubility [40] and promote foam expansion [24,41], or lead to negligible changes in foamability [33]. The present result may be rationalized by considering that, at the given temperature, the higher pressures can either be responsible for cell wall rupture during excessive bubble growth, upon the rapid decompression, or cause a stronger plasticization effect, due to the increasingly high gas uptake [40], possibly leading to the premature collapse of the foam structure. Further investigation is required to clarify this mechanism, which lies beyond the scope of the present work.

The effect of PDR is shown in Fig. 4(b). The foaming temperature and pressure were again selected based on the previously reported analysis (134 °C and 120 bar), while the investigated PDR values ranged from 50 to 933 bar/s. Again, while the neat TPU is not significantly affected by the PDR, the neat 3D printed and loaded preforms show a decreasing foam density with increasing PDR, in agreement with literature reports [42]. Overall, the results indicate that higher PDR values promote foam expansion, with the best PDR being at the upper end of the investigated range.

3.1.4. Foam morphology characterization

Fig. 5 shows the foam morphology of the TPU samples at different foaming temperatures. Overall, at the lowest temperature, small and well-defined bubbles are visible. As the foaming temperature increases, the bubble average size gradually increases, while the overall bubble number density decreases (see Supplementary, Figure SI 2), until the structure eventually collapses. This morphological evolution is consistent with the density reduction trends reported in Fig. 3, confirming that temperature strongly governs the balance between bubble growth and structural stability.

Despite the general behavior being similar, the evolution of the morphology with temperature presents significant differences when switching from one preform to another. Indeed, the presence of crystalline domains strongly influences the cell density and expansion ratio of the foams [20,21,23]. As previously discussed, each preform exhibits a distinct microstructure determined by its specific processing history,

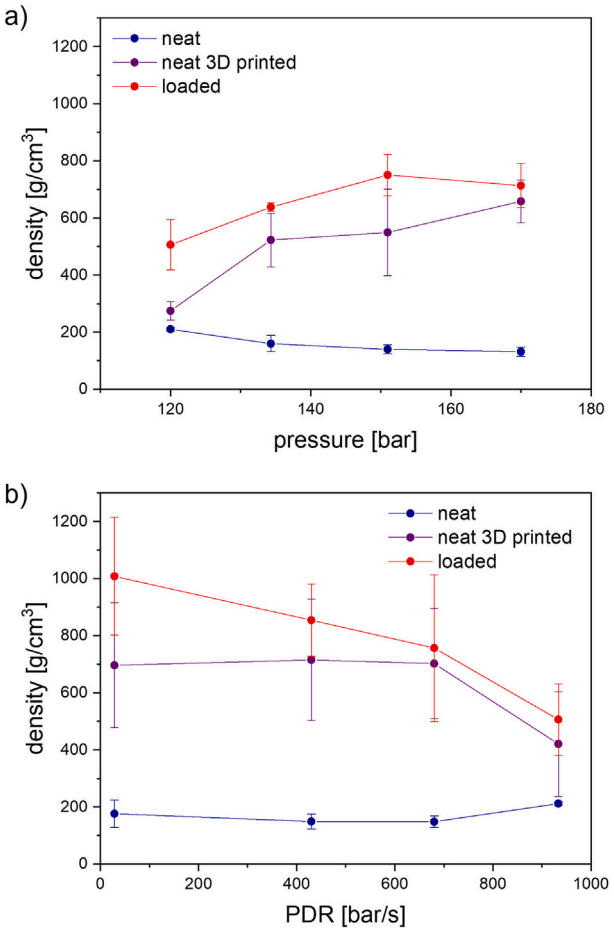

Fig. 4. Effect of foaming (a) pressure and (b) PDR on density reduction for different preforms processed by batch foaming at 134 °C using 933 bar/s and 120 bar of CO_2.

and these features are not completely erased during foaming, which explains the differences in foamability and foam morphology observed among the different preforms (Figs. 3 and 5).

The neat preform exhibits the most ordered crystalline structure, as indicated by the higher melting temperature in the DSC curves. According to literature, this favors bubble formation at lower temperatures due to a reduced nucleation barrier associated with heterogeneous nucleation on well-developed crystalline surfaces [21,43]. This ordered morphology is preserved during foaming at temperatures up to 134 °C, as evidenced by the microphotographs of Fig. 5.

In contrast, the neat 3D printed preform displays a finer and less ordered crystalline morphology (Fig. 1), thus determining the production of foams with smaller average bubble diameters [44] (Figure SI 2a), reduced expansion ratio (Fig. 3) and increased cell density (Figure SI 2b). This morphology can also be attributed to differences in CO_2 solubility: the lower fraction of crystalline HSs during processing determines a higher CO_2 solubility in the 3D printed preforms, as the gas molecules dissolve less readily in crystalline domains [19]. This, in turn, increases cell nucleation, contributing to the observed foam structures (Figure SI 2b) [24].

At high temperature, the process can be compared to an annealing process, the crystalline HSs with lower degree of perfection dissociate resulting in an enhanced polymer chain mobility that facilitates cell growth [45], but also cell rupture and coalescence due to the absence of unmelted HSs crystalline phase [23]. This explains the premature collapse observed in the neat 3D printed preforms at 155 °C (Fig. 5), which results in reduced foamability [20].

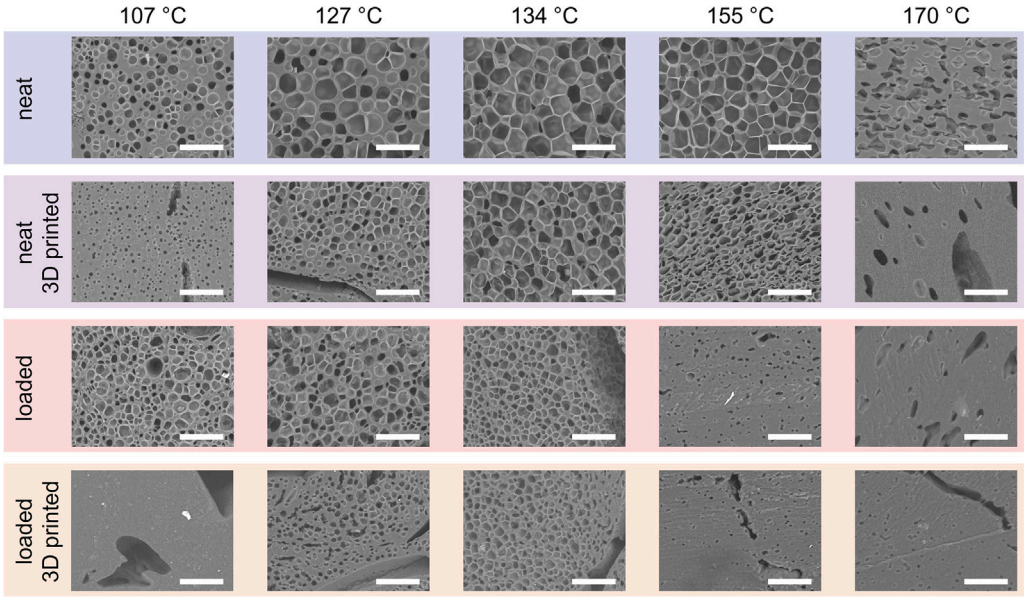

Fig. 5. SEM images of the cross section of the samples processed at diverse foaming temperatures. Scale bar 50 μm.

Regarding the loaded preforms, when foamed at lower temperatures, they exhibit a larger bubble number density (Figure SI 2b) with respect to the non-loaded ones, likely due to the heterogeneous nucleating effect of the fillers and the lower ΔH (i.e., lower overall crystallinity), while the reduced expansion and bubble average diameter (Figure SI 2a) may be related to the increase in the viscosity (Fig. 2).

The loaded 3D printed preforms' foamability closely resembles that of the loaded TPU, but with a narrower foaming window, as also observed in the comparison between neat TPU and neat 3D printed TPU. In this case, the higher fraction of crystalline phase (Fig. 1a) severely reduces gas solubility, as also evidenced by the absence of bubbles at 107 °C.

Interestingly, at 134 °C, all samples show a similar overall density reduction, but present different morphologies. The loaded preforms have a higher bubble number density, again confirming the combined role of the solubility change and the nucleating effect of the filler.

3.1.5. Foam shrinkage analysis

Foam shrinkage behavior was evaluated by measuring the density reduction seven days after foaming, when the sample's volume reached equilibrium. As shown in Fig. 6, ρ_{shrink} is always higher than ρ_{foam}.

In the case of the neat sample, a significant shrinkage is reported, especially at the lowest densities. A reduced shrinkage is reported in the case of the neat 3D printed preforms, (Fig. 6b), even at densities similar to those of the neat counterparts (which here occurs in the range 130–140 °C). This may be related to the different microstructures of the two preforms that may affect mechanical properties [46] and gas diffusivity, specifically reducing the effect of the counterpressure within the bubbles [47]. The loaded preforms display a more stable structure and the shrinkage appears to be non-proportional to the expansion ratio, unlike the neat TPU case (Fig. 6c). The loaded 3D printed preforms show a similar behavior, but with an overall reduced shrinkage, as already observed when comparing neat TPU and neat 3D printed TPU.

With the aim of quantifying the conditions at which minimum shrinkage is obtained, and to better compare these results, the SR was evaluated (Fig. 7). In all cases, a non-monotonic evolution of the SR is visible, with a significant increase in the range 140–160°C for the neat preform, i.e., when the foam has the lowest density [41]. The increase in the SR is lower for the neat 3D printed preform, for which shrinkage is never greater than 33%. The SR is even smaller for the loaded preforms: at 135 °C, a minimum in the SR value is observed, despite a density reduction comparable to that observed at lower temperatures. However, differently from the neat comparison, in the loaded case, the temperature dependence of the SR is quite similar in both the non-printed and the printed preforms. This is not valid, as anticipated, in the neat case, where a shift in the maximum SR is evident, probably reflecting the shift in the temperature at which the minimum density is detected (Fig. 3).

Overall, the lowest after shrinkage density is obtained by the neat TPU preforms, with values ρ_{shrink} as low as 308 ± 85 kg/m^3; however, from an application point of view, the after-shrinkage neat TPU cannot be considered the best sample as the significant shrinkage (evidenced by the high SR at the temperature where the minimum density is detected) causes the deformation of the as foamed sample geometry. The neat 3D-printed preforms, on the other hand, despite showing a higher minimum density (418 ± 31 kg/m^3), demonstrate superior dimensional stability, exhibiting very limited shrinkage. For functional applications where dimensional stability is critical, processing conditions where shrinkage is negligible are to be adopted.

3.2. Effect of pre-processing conditions

The effect of the 3D printing process on the foamability of the preforms is herein explored. 3D printing processing parameters include nozzle and filament size, printing temperature, printing speed, layer orientation, layer thickness, infill density and infill pattern [48]. However, among these, only a few affect the state of the printed polymer. Indeed, parameters like infill and layer thickness essentially determine the geometry and internal architecture of the printed part without directly affecting the thermal and deformation history of the material. Accordingly, we will focus on only two printing parameters, namely T_{print} and v_{print}, as the primary variables influencing the residual stresses and crystalline structure within the final piece [49–51], hence bridging the gap between processing-induced thermal history and the morphological characteristics of the foamed polymer.

3.2.1. Printing temperature

The printing temperature corresponds to the hot end temperature during the printing process. From a materials perspective, varying the printing temperature alters the thermal history experienced by both the deposited and the underlying filaments, thereby affecting the crystallinity buildup of the material [52], as evident from the rheological

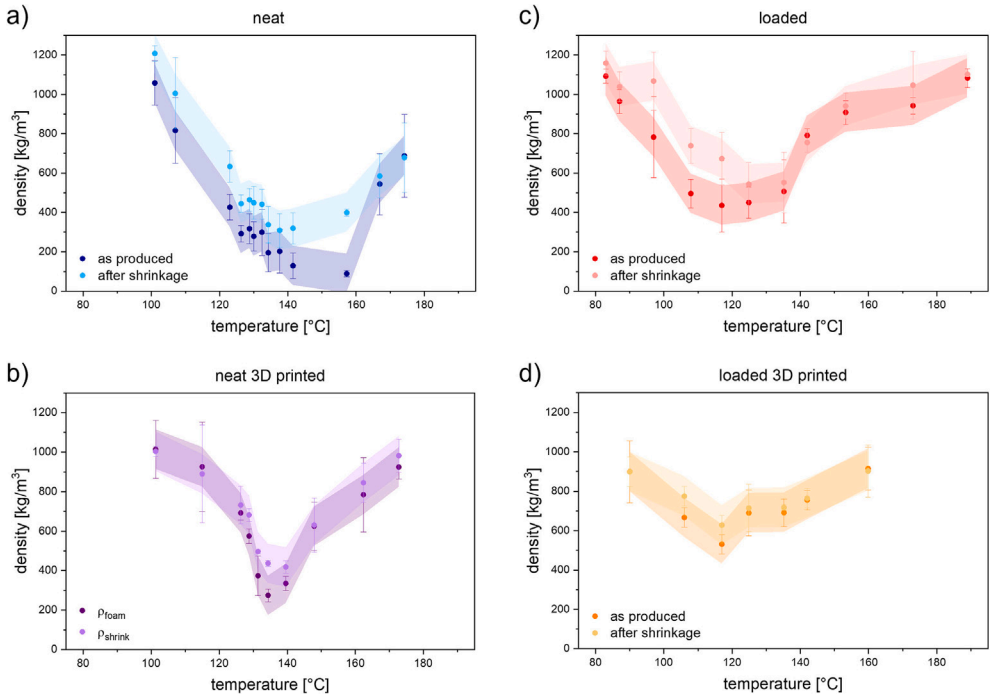

Fig. 6. Density reduction as a function of temperature right after foaming ρ_{foam} and after shrinkage ρ_{shrink} for each preform type, namely (a) neat TPU pellets, (b) neat TPU 3D printed samples, (c) loaded TPU, (d) loaded TPU 3D printed samples.

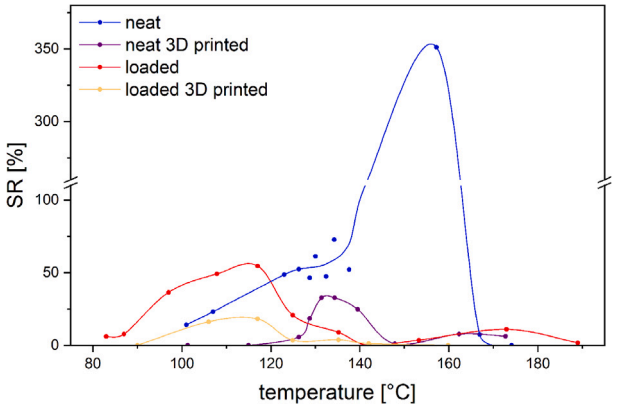

Fig. 7. Shrinkage ratio (SR) as a function of the foaming temperature for each preform type, namely (a) neat TPU pellets, (b) neat TPU 3D printed samples, (c) loaded TPU, (d) loaded TPU 3D printed samples; the lines are a guide to the eye.

study (Figure SI 1a) and the DSC curves collected prior to foaming (Figure SI 3a).

These microstructural differences are reflected in the foamability of the samples, as depicted in Fig. 8(a), where the density of the foamed preforms printed at temperatures ranging from 195 °C to 225 °C is reported. Notably, all samples were foamed under the previously identified optimal conditions (134 °C, 120 bar CO_2, and a PDR of 933 bar/s).

As the printing temperature increases, the foamability decreases, as evidenced by the higher density of the resulting foams. Accordingly, the most suitable printing temperature can be identified as 195 °C. Overall, the influence of printing temperature is significant, leading to a density variation of approximately 270 kg/m^3, which confirms a strong sensitivity of the foaming behavior to the thermal history imposed during the printing stage.

3.2.2. *Printing speed*

The printing speed affects both the residence time of the filament within the hot end and nozzle, as well as the shear stress to which the molten polymer is subjected. Samples printed at velocities ranging from 10 mm/s to 30 mm/s were foamed under the previously identified optimal conditions (134 °C, 120 bar CO_2, and a PDR of 933 bar/s). For each sample, the final foam density was measured, as reported in Fig. 8(b). A slight decrease in density is observed with increasing printing speed, suggesting a marginal improvement in foamability. However, considering the experimental variability and reproducibility, this effect is negligible. It can therefore be concluded that foamability is not significantly influenced by printing speed, and the optimal printing speed may be selected based on other processing considerations.

3.3. *Toward advanced applications*

When a material undergoes free and uniform expansion, the initial geometry is faithfully reproduced on a large scale. However, when local differences in expansion are induced, they can result in non-trivial deformation effects, that, in turn, can determine a significant change in the geometry of the final product. Exploiting the shape change can be envisioned as *morphing* [53,54]. In the present paragraph, we explore how the accurate design of the sample preform can be exploited as a way to induce morphing in mold-free batch foaming.

Indeed, by tailoring the 3D printing parameters and/or combining differently processed filaments (e.g., filaments printed at different T_{print} or v_{print}, or neat and loaded filaments) in the printed geometry, we can modulate the local expansion. In other words, the evolution of the sample can be virtually predetermined within the preform prior to foaming, enabling the exploitation of foaming itself as a morphing trigger [49,51,55]. We will herein call this mechanism *Foam Induced Morphing*.

To explore and demonstrate the feasibility of this method, we first present proof-of-concept structures designed to qualitatively demonstrate morphing upon foaming. We processed two different scaled-up 3D printed architectures, which are shown in Fig. 9 . As visible, the first

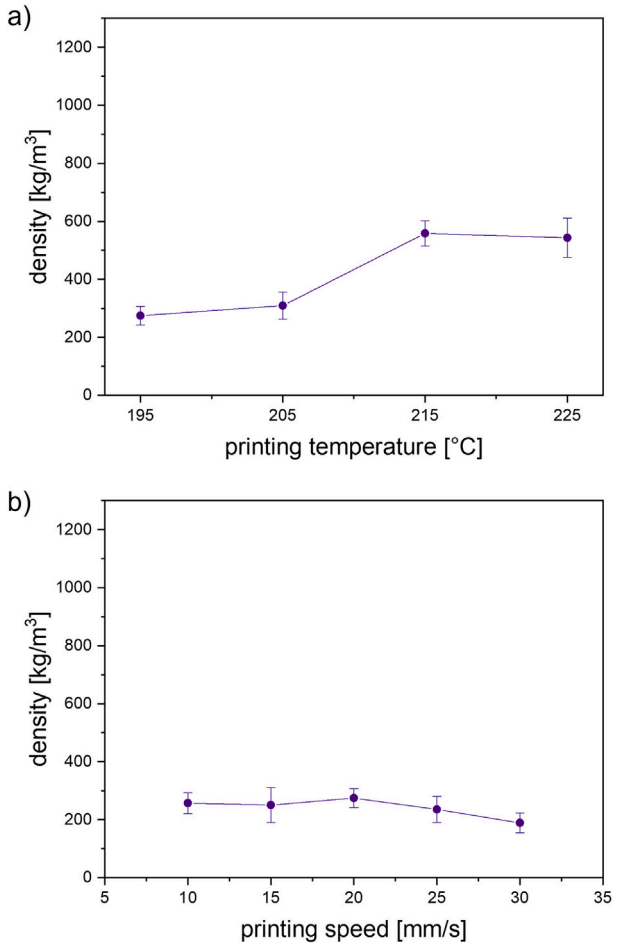

Fig. 8. Effect of 3D printing (a) temperature and (b) speed on density reduction of preforms processed by batch foaming at 134 °C, 120 bar of CO_2 and 933 bar/s.

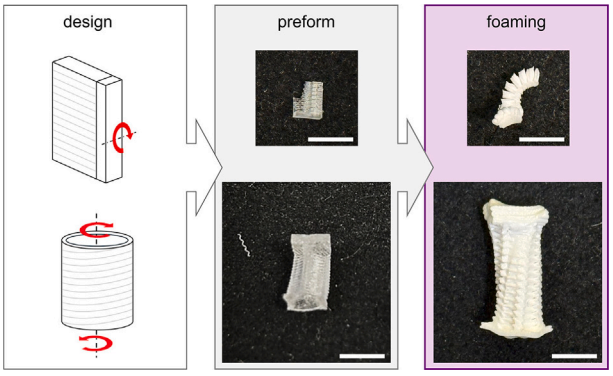

Fig. 9. Flow chart of foaming induced geometry morphing of neat 3D printed samples by design. Comparison of two different preforms with the respective final foam samples. The first design promotes the foaming induced bending (top), and the second promotes torsion induced foaming (bottom). Scale bar 0.5 cm.

preform, consisting of lamellae connected to a vertical truss, undergoes bending during foaming, as the expansion of the lamellae is constrained by the vertical element. The second preform, on the other hand, is a cylindrical element and undergoes torsional deformation upon foaming.

To move beyond qualitative observation and toward a more design-oriented strategy, we further demonstrate that foam-induced morphing can be programmed by combining preforms with intrinsically different expansion behaviors. Indeed, one can thus exploit, through foaming, their intrinsic ability to expand to a different extent under identical foaming conditions (as presented in Section 3.1.3, Fig. 4 and Section 3.2), enabling production of non-trivial final foamed shapes.

An example of this second approach is reported in Section 3.2, in which a two layer preform produced by combining layers printed at 225 °C (bottom half) and layers printed at 195 °C (top half) is presented. By exploiting the wide difference in foamability of the two halves, reported in Section 3.2, possibility of obtaining foam induced morphing is foreseen.

The problem is quite complex as the foaming process involves the treatment of the polymer at high temperature for a sufficiently long time to allow the solubilization of the blowing agent (t_{sat}) before the pressure drop can be applied. As a consequence, the first effect of this process is thermal shrinkage, which causes the filament to recover the strain induced during the filament deposition. This effect is well reported in the literature [49,51] and is enough to induce shape morphing when combined with a precise printing pattern design [56,57].

To quantify heat-induced morphing during our process, we monitored the length L of two filament pieces printed at T_{print} = 195 °C and T_{print} = 225 °C, respectively, during heating from 20 to 134 °C (this being the optimal foaming temperature identified in Section 3.1.3 for a neat 3D printed preform). The thermal shrinkage $(L - L_0)/L_0$ as a function of time and temperature is presented in Fig. 10(a). As illustrated, the filament length decreases with rising temperature, and the magnitude of this contraction is highly sensitive to pre-processing conditions, again highlighting the possibility of exploiting pre-processing to induce changes in the 3D printed parts, even without the need for complex printing pattern design. Specifically, length reductions of 39.5% and 12% were observed for T_{print} values of 195 °C and 225 °C, respectively. This behavior was also confirmed by foaming experiments conducted on the two-layer preform. The primary morphing induced by heat caused a retraction of the two layers which was found to be consistent with the shrinkage data obtained from the individual filaments printed at those respective temperatures (higher shrinkage when at lower T_{print}), as evidenced in Fig. 10(b).

When the pressure is finally dropped, a secondary foam-induced morphing occurs (Fig. 10c). Since expansion depends on the printing temperatures, as detailed in Section 3.2.1, a non-isotropic expansion is detected. This is confirmed by evaluating the ratio of the lengths of the two parts, which is not maintained after foaming, as would have happened in an isotropic expansion. Before foaming, it is 2.14, while after foaming, it decreases to 1.18; hence, it is reduced to half of its original value. This is consistent with the results of Fig. 8, in which a lower expansion of the layer printed at 225 °C is expected with respect to that printed at 195 °C. The relative expansion ratio of almost 0.5 ultimately causes the material to bend in the opposite direction of the heat-induced curvature. This change indicates that the foaming process effectively 'retrieves' or compensates for the prior shrinkage through localized expansion. Precise calibration of this phenomenon, accounting for the localized density variations in each component, offers a robust, unprecedented framework for a novel approach to programmable morphing.

Although there is still much to explore and refine, these examples demonstrate how preform design and material pre-processing, combined with the freedom of a mold-free foaming process, can be effectively employed to encode and trigger shape transformations, introducing a new paradigm of foam-induced morphing in polymeric systems.

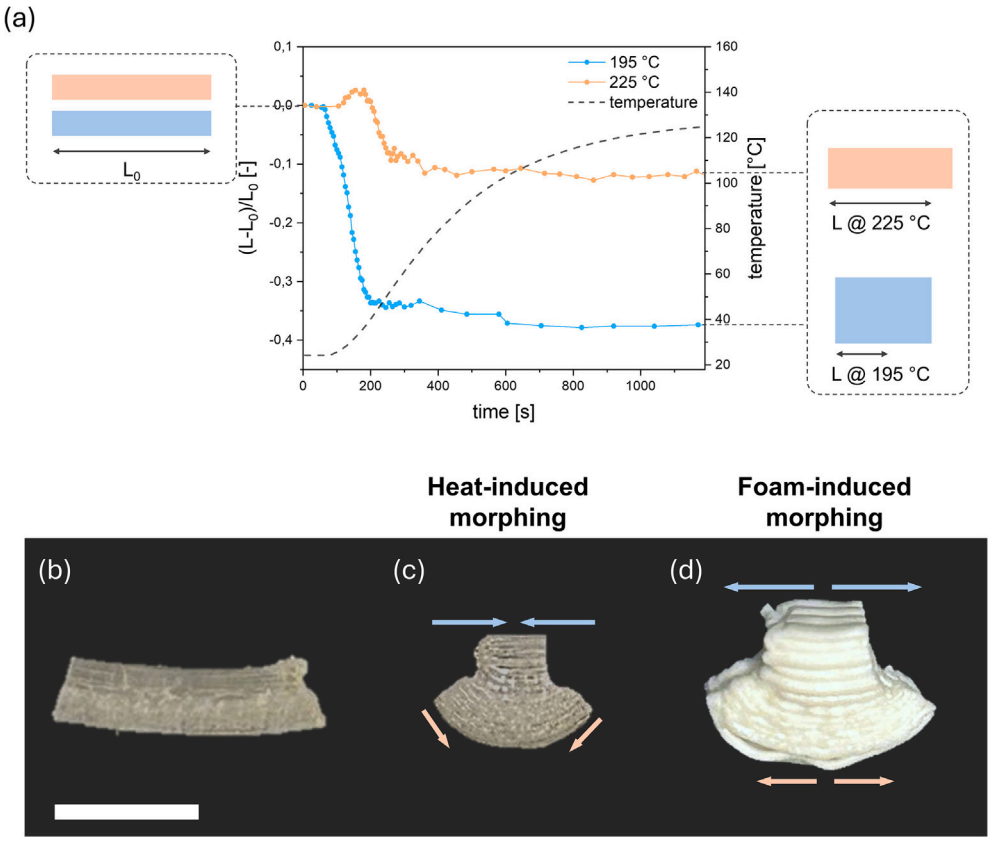

Fig. 10. (a) evolution of the heat-induced thermal shrinkage of two TPU filaments printed at 195 (light blue) and 225 °C (light orange) as a function of time and temperature, and bi-layer preform (top half printed at 195 °C, bottom half printed at 225 °C) before foaming (b), after heating (c) and after foaming. The scale bar corresponds to 0.5 mm.

4. Conclusions

This work demonstrates that the foamability of thermoplastic polyurethane processed by supercritical CO_2 is not solely governed by foaming parameters but is strongly affected by the pre-processing history of the material. By systematically comparing neat, 3D printed, loaded, and 3D printed loaded preforms, we establish a direct link between pre-processing, microstructural state, and subsequent expansion, morphology, and shrinkage behavior. The results show that microstructural modifications introduced during 3D printing are not erased during foaming but instead actively determine bubble nucleation, growth, and structural stability.

Both neat and loaded 3D-printed samples showed limited density reduction, attributed primarily to microstructural influences on gas transport and bubble nucleation. Filler incorporation enhanced structural stability, mitigating shrinkage and shifting the foaming window to lower temperatures (108–135 °C).

Regarding printing parameters, printing speed had a negligible effect, whereas elevated printing temperatures significantly reduced TPU foamability.

Building on this understanding, we introduce and experimentally validate the concept of *foam-induced morphing*. By integrating regions printed under distinct thermal histories, non-isotropic growth is triggered under uniform foaming conditions, enabling predictable non-isotropic shape transformation. The decoupled analysis of heat-induced shrinkage and subsequent foam-induced expansion confirms that shape evolution can be encoded at the deposition stage and activated during foaming. These findings position mold-free batch foaming as a design tool for programmable, shape-transforming polymer architectures. The combined control of 3D printing and supercritical CO_2 batch foaming parameters opens new opportunities for tailored lightweight systems with tunable mechanical responses and controlled morphing behavior, toward applications in advanced fields like soft robotics.

CRediT authorship contribution statement

Lorenzo Miele: Writing – review & editing, Writing – original draft, Visualization, Validation, Methodology, Investigation, Formal analysis, Data curation, Conceptualization. **Emilia Di Lorenzo:** Writing – review & editing, Writing – original draft, Visualization, Validation, Methodology, Investigation, Formal analysis, Data curation, Conceptualization. **Denise Bellisario:** Writing – review & editing, Supervision, Resources, Project administration, Funding acquisition. **Ernesto Di Maio:** Writing – review & editing, Writing – original draft, Supervision, Resources, Conceptualization.

Funding

This research was funded by the Research Projects of Significant National Interest (PRIN) 2022, project no. 2022SFF349, with CUP Master D53D23004020008 within the project named “4D Printing of Smart Soft Robotics (4D P.Ro.)”.

Declaration of competing interest

The authors declare that they have no known competing financial interests or personal relationships that could have appeared to influence the work reported in this paper.

Acknowledgments

The authors thank Rossana Pasquino (University of Naples Federico II) for the support provided in performing the rheological characterization reported in Fig. 2.

Appendix A. Supplementary data

Supplementary data for this article can be found online at doi:10.1016/j.matdes.2026.115852.

Data availability

Data will be made available on request.

References

[1] W. Zhai, J. Jiang, C.B. Park, A review on physical foaming of thermoplastic and vulcanized elastomers, Polym. Rev. 62 (1) (2022) 95–141.
[2] Y. Gu, Z. Xu, F. Fan, L. Wei, T. Wu, Q. Li, Highly breathable, stretchable, and tailorable TPU foam for flexible gas sensors, ACS Sens. 8 (10) (2023) 3772–3780.
[3] A. Mohammadi, J. Lavranos, H. Zhou, R. Mutlu, G. Alici, Y. Tan, P. Choong, D. Oetomo, A practical 3D-printed soft robotic prosthetic hand with multi-articulating capabilities, PLoS One 15 (5) (2020) e0232766.
[4] D. Rus, M.T. Tolley, Design, fabrication and control of soft robots, Nature 521 (7553) (2015) 467–475.
[5] Y. Chen, H. Chung, B. Chen, Y. Sun, et al., A lobster-inspired bending module for compliant robotic applications, Bioinspir. Biomim. 15 (5) (2020) 056009.
[6] A.N.J. Spörrer, V. Altstädt, Controlling morphology of injection molded structural foams by mold design and processing parameters, J. Cell. Plast. 43 (4–5) (2007) 313–330.
[7] A.N.J. Spoerrer, D.S. Bangarusampath, V. Altstaedt, The challenge of foam injection-moulding–possibilities to improve surface appearance, foam morphology and mechanical properties, Cell. Polym. 27 (2) (2008) 101–121.
[8] D. Raps, N. Hossieny, C.B. Park, V. Altstädt, Past and present developments in polymer bead foams and bead foaming technology, Polymer 56 (2015) 5–19.
[9] J. Minguella-Canela, S.M. Planas, J.R.G. Ayats, M.A. De los Santos López, Study and comparison of the different costs' schema associated to geometry, material and processing between 3D printing, injection molding and machining manufacturing technologies, Proc. Manuf. 41 (2019) 280–287.
[10] X. Jiang, L. Zhao, L. Feng, C. Chen, Microcellular thermoplastic polyurethanes and their flexible properties prepared by mold foaming process with supercritical CO_2, J. Cell. Plast. 55 (6) (2019) 615–631.
[11] L. Miele, A. Abate, K. Taki, E. Di Maio, Bubble dynamics manipulation in polymeric foaming, Soft Matter 20 (44) (2024) 8845–8854.
[12] Y.-G. Zhou, T.-Y. Chen, Combining foam injection molding with batch foaming to improve cell density and control cellular orientation via multiple gas dissolution and desorption processes, Polym. Adv. Technol. 31 (10) (2020) 2136–2151.
[13] H. Liu, C. Wu, S. Lin, J. Lam, N. Xi, Y. Chen, Advances in 3D and 4D printing of soft Robotics and their applications, Adv. Intell. Syst. 7 (6) (2025) 2400699.
[14] A. Longo, D. Giannetti, D. Tammaro, S. Costanzo, E. Di Maio, TPU-based porous heterostructures by combined techniques, Int. Polym. Process. 37 (4) (2022) 415–426.
[15] Z.S. Petrović, J. Ferguson, Polyurethane elastomers, Prog. Polym. Sci. 16 (5) (1991) 695–836.
[16] R.M. Briber, E.L. Thomas, Investigation of two crystal forms in mdi/bdo-based polyurethanes, J. Macromol. Sci, Part B: Phys. 22 (4) (1983) 509–528.
[17] J. Balko, B. Fernández-d'Arlas, E. Poselt, R. Dabbous, A.J. Muller, T. Thurn-Albrecht, Clarifying the origin of multiple melting of segmented thermoplastic polyurethanes by fast scanning calorimetry, Macromolecules 50 (19) (2017) 7672–7680.
[18] P.J. Yoon, C.D. Han, Effect of thermal history on the rheological behavior of thermoplastic polyurethanes, Macromolecules 33 (6) (2000) 2171–2183.
[19] J.H. Lee, S.H. Mahmood, J.-M. Pin, R. Li, P.C. Lee, C.B. Park, Determination of CO_2 solubility in semi-crystalline polylactic acid with consideration of rigid amorphous fraction, Int. J. Biol. Macromol. 204 (2022) 274–283.
[20] N.J. Hossieny, M.R. Barzegari, M. Nofar, S.H. Mahmood, C.B. Park, Crystallization of hard segment domains with the presence of butane for microcellular thermoplastic polyurethane foams, Polymer 55 (2) (2014) 651–662.
[21] K. Taki, D. Kitano, M. Ohshima, Effect of growing crystalline phase on bubble nucleation in poly (l-lactide)/CO_2 batch foaming, Ind. Eng. Chem. Res. 50 (6) (2011) 3247–3252.
[22] Y. Yang, X. Li, Q. Zhang, C. Xia, C. Chen, X. Chen, P. Yu, Foaming of poly (lactic acid) with supercritical CO_2: the combined effect of crystallinity and crystalline morphology on cellular structure, J. Supercrit. Fluids 145 (2019) 122–132.
[23] B. Chen, J. Jiang, Z. Wang, Y. Li, F. Tian, L. Wang, W. Zhai, Controlling the crystal morphology of high-hardness TPU through two pre-crystallization processes and its impact on physical foaming behavior, Polymer 305 (2024) 127172.
[24] M. Nofar, E.B. Küçük, B. Batı, Effect of hard segment content on the microcellular foaming behavior of TPU using supercritical CO_2, J. Supercrit. Fluids 153 (2019) 104590.
[25] A. Deshpande, A. Ravi, S. Kusel, R. Churchwell, K. Hsu, Interlayer thermal history modification for interface strength in fused filament fabricated parts, Prog. Addit. Manuf. 4 (1) (2019) 63–70.
[26] B. Redwood, F. Schffer, B. Garret, The 3D Printing Handbook: Technologies, Design and Applications, 3D Hubs, 2017.
[27] M. Roy, O. Wodo, Data-driven modeling of thermal history in additive manufacturing, Addit. Manuf. 32 (2020) 101017.
[28] S. Khan, K. Joshi, S. Deshmukh, A comprehensive review on effect of printing parameters on mechanical properties of FDM printed parts, Mater. Today Proc. 50 (2022) 2119–2127.
[29] C. Marrazzo, E. Di Maio, S. Iannace, Conventional and nanometric nucleating agents in poly (ϵ-caprolactone) foaming: crystals VS. Bubbles nucleation, Polym. Eng. Sci. 48 (2) (2008) 336–344.
[30] X. Gao, Y. Chen, P. Chen, Z. Xu, L. Zhao, D. Hu, Supercritical CO_2 foaming and shrinkage resistance of thermoplastic polyurethane/modified magnesium borate whisker composite, J. CO_2 Util. 57 (2022) 101887.
[31] L. Monnereau, L. Urbanczyk, J.-M. Thomassin, M. Alexandre, C. Jérôme, I. Huynen, C. Bailly, C. Detrembleur, Supercritical CO_2 and polycarbonate based nanocomposites: a critical issue for foaming, Polymer 55 (10) (2014) 2422–2431.
[32] L. Burratti, D. Bellisario, F. Quadrini, L. Iorio, L. Santo, 3D printing of soft actuators in nano-filled shape memory thermoplastic polyurethane, Mater. Res. Proc. 54 (2025).
[33] L. Miele, E. Di Lorenzo, C. Guissart, E. Di Maio, Liquid foaming of TPU with methylal, Heliyon 10 (12) (2024).
[34] C.A. Schneider, W.S. Rasband, K.W. Eliceiri, Nih image to imagej: 25 years of image analysis, Nat. Methods 9 (7) (2012) 671–675.
[35] Z. Wang, X. Li, E. Pöselt, B. Eling, T. Liao, Z. Wang, Polymorphic microstructure of mdi/bd-block polyurethane as determined by temperature-sensitive conformation variation, Soft Matter 17 (41) (2021) 9447–9456.
[36] R.W. Seymour, S.L. Cooper, DSC studies of polyurethane block polymers, J. Polym. Sci. Part B Polym. Lett. 9 (9) (1971) 689–694.
[37] F. Liu, X. Liao, Q. Peng, Y. Zhao, S. Li, G. Li, Effect of two crystalline forms on the multiple melting and crystallization kinetics of thermoplastic polyurethane, Cryst. Growth Des. 22 (10) (2022) 6015–6022.
[38] L.M. Leung, J.T. Koberstein, DSC annealing study of microphase separation and multiple endothermic behavior in polyether-based polyurethane block copolymers, Macromolecules 19 (3) (1986) 706–713.
[39] M.R. Barzegari, N. Hossieny, D. Jahani, C.B. Park, Characterization of hard-segment crystalline phase of poly (ether-block-amide)(PEBAX®) thermoplastic elastomers in the presence of supercritical CO_2 and its impact on foams, Polymer 114 (2017) 15–27.
[40] R. Li, J.H. Lee, C. Wang, L.H. Mark, C.B. Park, Solubility and diffusivity of CO2 and N2 in tpu and their effects on cell nucleation in batch foaming, J. Supercrit. Fluids 154 (2019) 104623.
[41] D. Zhao, G. Wang, M. Wang, Investigation of the effect of foaming process parameters on expanded thermoplastic polyurethane bead foams properties using response surface methodology, J. Appl. Polym. Sci. 135 (25) (2018) 46327.
[42] D. Tammaro, S. Iannace, E. Di Maio, Insight into bubble nucleation at high-pressure drop rate, J. Cell. Plast. 53 (5) (2017) 551–560.
[43] A. Wong, Y. Guo, C.B. Park, Fundamental mechanisms of cell nucleation in polypropylene foaming with supercritical carbon dioxide—effects of extensional stresses and crystals, J. Supercrit. Fluids 79 (2013) 142–151.
[44] C. Niu, X. Gao, Y. Chen, W. Sun, L. Zhao, D. Hu, Supercritical CO_2 foaming and mechanical properties of thermoplastic polyurethane based on molecular structure, J. Supercrit. Fluids 219 (2025) 106541.
[45] H.E. Naguib, C.B. Park, N. Reichelt, Fundamental foaming mechanisms governing the volume expansion of extruded polypropylene foams, J. Appl. Polym. Sci. 91 (4) (2004) 2661–2668.
[46] M. Amirkhosravi, L. Yue, T. Ju, I. Manas-Zloczower, Designing thermal annealing to control mechanical performance of thermoplastic polyurethane elastomers, Polymer 214 (2021) 123254.
[47] A. Puentes-Parodi, L.A. Santoro, I. Ferreira, A. Leuteritz, I. Kuehnert, Influence of annealing on the permeation properties of a thermoplastic elastomer, Polym. Eng. Sci. 59 (9) (2019) 1810–1817.
[48] M.M. Prabhakar, A.K. Saravanan, A.H. Lenin, K. Mayandi, P.S. Ramalingam, et al., A short review on 3D printing methods, process parameters and materials, Mater. Today Proc. 45 (2021) 6108–6114.
[49] T. Van Manen, S. Janbaz, A.A. Zadpoor, Programming 2D/3D shape-shifting with hobbyist 3D printers, Mater. Horiz. 4 (6) (2017) 1064–1069.
[50] N. Schiavone, V. Verney, H. Askanian, Effect of 3D printing temperature profile on polymer materials behavior, 3D Print. Addit. Manuf. 7 (6) (2020) 311–325.
[51] G. Wang, H. Yang, Z. Yan, N. Gecer Ulu, Y. Tao, J. Gu, L.B. Kara, L. Yao, 4Dmesh: 4D printing morphing non-developable mesh surfaces, in: Proceedings of the 31st Annual ACM Symposium on User Interface Software and Technology, 2018, pp. 623–635.
[52] C. Yang, X. Tian, D. Li, Y. Cao, F. Zhao, C. Shi, Influence of thermal processing conditions in 3D printing on the crystallinity and mechanical properties of PEEK material, J. Mater. Process. Technol. 248 (2017) 1–7.
[53] H. Quan, D. Kisailus, M.A. Meyers, Hydration-induced reversible deformation of biological materials, Nat. Rev. Mater. 6 (3) (2021) 264–283.
[54] Y. Tao, Y.-C. Lee, H. Liu, X. Zhang, J. Cui, C. Mondoa, M. Babaei, J. Santillan, G. Wang, D. Luo, et al., Morphing pasta and beyond, Sci. Adv. 7 (19) (2021) eabf4098.
[55] S.A. Chester, C.V. Di Leo, L. Anand, A finite element implementation of a coupled diffusion-deformation theory for elastomeric gels, Int. J. Solids Struct. 52 (2015) 1–18.
[56] J. Leng, X. Lan, Y. Liu, S. Du, Shape-memory polymers and their composites: stimulus methods and applications, Prog. Mater. Sci. 56 (7) (2011) 1077–1135.
[57] K. Oliver, A. Seddon, R.S. Trask, Morphing in nature and beyond: a review of natural and synthetic shape-changing materials and mechanisms, J. Mater. Sci. 51 (24) (2016) 10663–10689.